

The Use of Soft X-ray Spectromicroscopy to Investigate the Distribution and Composition of Organic Matter in a Diatom Frustule and a Biomimetic Analog

Lynn Abramson¹ Sue Wirick², Cindy Lee^{1*}, Chris Jacobsen², Jay A. Brandes³

1. School of Marine and Atmospheric Sciences, Stony Brook University, Stony Brook, NY 11794-5000
2. Department of Physics and Astronomy, Stony Brook University, Stony Brook, NY 11794-3800
3. Skidaway Institute of Oceanography, 10 Ocean Sciences Circle, Savannah, GA 31411-1011

* Author to whom correspondence should be addressed (cindylee@notes.cc.sunysb.edu; fax: 631-632-8820)

Abstract

Diatoms are common marine algae that play a significant role in the global carbon cycle through their role in biogenic silica production and the transport of organic matter to the seafloor. Recent work has shown that silicified cell walls, or frustules, of diatoms contain a significant amount of organic matter, and that the proportion of diatom-bound organic matter increases with depth in the water column and sediments. Here we investigate the association between organic matter and the mineral phase. We used a combination of scanning transmission X-ray microscopy (STXM) and carbon X-ray absorption near-edge structure (XANES) spectroscopy to characterize the distribution and composition of organic matter in frustules of the diatom *Cylindrotheca closterium* and a biomimetic silica gel. To our knowledge, this study represents the first successful attempt to simultaneously image and obtain chemical information about the organic matter within a diatom frustule using X-ray spectromicroscopy near the carbon edge. Organic carbon, most likely protein, was distributed throughout the frustules and was not removed by harsh chemical treatment. The physical structure of the frustules appeared to be related to the chemical composition of this organic matter, with aromatic or unsaturated carbon being concentrated in the most intricately patterned regions of the frustule. A similar physical and chemical structure was observed in a biomimetic silica gel precipitated spontaneously with polylysine. These results are consistent with the theory that organic constituents of diatom frustules direct silica precipitation and become incorporated within the silica matrix as it forms. The relationship between organic matter composition and silica morphology, the failure of harsh chemical treatments to remove this organic matter, and the spontaneous nature of the co-precipitation of silica and organic matter indicate some chemical interaction between the siliceous and organic components of diatom frustules. Frustule-bound organic matter should therefore be protected from decomposition in the water column or diagenetic alteration in sediments unless the frustule dissolves.

Keywords: diatom frustules, organic matter, degradation, minerals, preservation

1. Introduction

The ratio of particulate organic carbon to mineral ballast converges to a nearly constant value ($\sim 3\text{-}7$ wt% POC) in particles sinking below 1800 m depth in the ocean, implying a strong association between organic carbon and mineral material (Armstrong et al., 2002; Klaas and Archer, 2002). Diatoms are common marine algae that play a significant role in the global carbon cycle through their role in biogenic silica production and the transport of organic matter to the seafloor. They produce an intricately-patterned silicified cell wall known as a frustule, which itself contains organic constituents that contribute to the export of carbon from the surface ocean. In addition to organic coatings on the outer or inner surfaces of the frustule (Round et al., 1990), some organic matter appears to be bound within the mineral structure itself, comprising up to 0.2 wt% of the shell, or 28 weight% of the entire cell wall (Hecky et al., 1973; Weiner and Erez, 1984). This organic matter consists primarily of silaffins, or proteins with sulfated polysaccharide side-chains (Kröger et al., 1999) as well as some polyamines (Kröger et al., 2000) and sugars (Hecky et al., 1973). It remains even after hydrolysis with HCl or chemical oxidation and is released only upon HF-dissolution of frustules (Swift and Wheeler, 1991; Kröger et al., 1999; Ingalls et al., 2003). Therefore, a substantial fraction of this biomineral-bound organic carbon may be protected from decomposition in the water column and sediments (King, 1974; Robbins and Brew, 1990; Ingalls et al., 2003). Even though this material represents only a small fraction of the total organic carbon in the ocean, it can represent a significant fraction of carbon in siliceous sediments.

Although organic components are known to be present within diatom frustules, their precise location and type of association with the silica frustule have not been characterized. It is not clear whether the organic constituents exist as a layer on the exterior or interior surface of the frustule, or

if they are located internally within the frustule itself, dispersed among the silica molecules. Also, the level of chemical interaction between the organic and siliceous components is unknown.

The extent to which organic components of the frustule are protected from decomposition likely depends on the nature of their association with silica. Consequently, understanding this association is important in predicting the contribution of frustule-bound organic matter to the biological carbon pump. In addition, this information is crucial for the interpretation of paleoceanographic tools such as the use of frustule-bound carbon to measure radiocarbon age in low-carbonate sediments (Ingalls et al. 2004) or the use of frustule-bound nitrogen isotopes as tracers of nutrient availability (Sigman et al. 1999). These techniques rely on the assumption that the organic matter within frustules undergoes no diagenetic alteration following its burial in sediments. Although some of the organic matter in frustules is clearly protected against such modification, it is still not certain how complete this protection is or what level of chemical association it requires.

Previous studies addressing the silicification mechanisms of diatoms provide some clues as to the nature of the association between organic matter and silica in frustules. In the diatom cell, solid deposits of silica are formed in organelles called silica deposition vesicles. As these silica deposits are arranged into the intricate patterning of the frustule, they remain intimately attached to the silicalemma, or membrane covering these vesicles (Li and Volcani, 1984). This suggests that the organic membrane acts as a template for silica deposition, possibly via hydrogen bonding or ionic interaction (Volcani, 1981), or condensation on the hydroxyl groups of serine and threonine (Hecky et al., 1973). Natural proteins and polyamines isolated from HF-dissolved frustules, as well as some synthetic polyamines, are capable of precipitating nanostructured silica when added to solutions of silicic acid, suggesting that the organic constituents of diatom frustules may direct patterns of silica deposition (Mitzutani et al., 1998; Kröger et al., 2000; Noll et al., 2002). This implies some degree of chemical interaction between the silica and organic matter in frustules. Recent studies using ^{29}Si -

NMR (e.g., Kinrade et al., 2002; Sahai, 2004) attempted to determine if silicon forms ester or ether-like complexes with organic molecules, but found that the dominant form in diatoms is monosilicic acid.

The objectives of this study were to elucidate 1) how the organic scaffold might influence silica precipitation in diatom frustules and 2) what fraction of the frustule-bound organic matter is protected against chemical attack. Specifically, we examined how organic constituents are distributed throughout the frustule of one diatom species and how this was altered by progressively more stringent levels of chemical attack. The distribution of organic matter entrapped within a silica gel was also investigated to elucidate whether the co-precipitation of organic and inorganic components occurs spontaneously and survives chemical attack. These goals were accomplished using chemical oxidation and hydrolysis techniques and soft X-ray spectromicroscopy, which simultaneously provided information on the physical structure of diatom frustules as well as the distribution and molecular composition of the organic matter within.

2. Methods

2.1. Sample preparation

We investigated the distribution and composition of organic matter in diatom frustules and a synthetic silica gel. The diatom *Cylindrotheca closterium* (also known as *Nitzschia closterium*) was selected because it was found to have a thin, spectrally transparent frustule. Attempts were made with other species as well (including several *Coscinodiscus* species and diatomaceous earth samples); however, the thick silica in these diatoms absorbed X-rays too strongly to determine whether carbon was present. *C. closterium* was isolated from a natural seawater sample and identified according to Tomas (1997) and Round et al. (1990). Cells were grown in batch culture (f/2 media with salinity 35.1 psu) at 15°C with a light flux of 100 $\mu\text{mol m}^{-2}\text{s}^{-1}$ in a 16h:8h light:dark cycle. The silica gel was prepared by

adding polylysine to a buffered solution of silicic acid and allowing the silica to precipitate overnight. Mitzutani et al. (1998), Kröger et al. (1999, 2000, 2002), and Noll et al. (2002) have previously used a similar approach, precipitating silica by adding natural or commercially available silaffins and polyamines to silicic acid. The synthetic silica is referred to here as a “gel” out of convention with previous research; however, it is important to note that the silica gel had more of a solid than gel-like appearance and retained its physical appearance even after drying.

Untreated diatoms were examined by light microscopy (1000X magnification) to determine the general structure of cells. The samples were then subjected to progressively more stringent levels of treatment (a surfactant, mild oxidant, and finally, strong acid) to elucidate the strength of the association between the organic matter and silica. Intracellular and surficial organic matter was first removed from the fresh *C. closterium* cultures (since it would mask spectroscopic signals from the frustule-bound organic matter) by freeze-lysing the diatoms and sonicating them for 30 min in 2:1 (CH₂)₂Cl₂:MeOH. Subsequent cleaning procedures (performed on both the diatoms and gel) included treatment with 30% H₂O₂ overnight and finally, with 6N HCl at 110°C for 20 h. Samples were rinsed three times with Milli-Q water following each cleaning procedure. Finally, each sample was resuspended in deionized water and a small drop was placed on a Si₃N₄ window (a 100-nm thick transparent film used to mount samples) and allowed to air-dry. This caused the sample to be distributed in a thin layer over the window.

In the initial development of these cleaning procedures, we checked for unrecovered amino acids after the final step (HCl hydrolysis) by performing a second hydrolysis as in Ingalls et al. (2003). Using high-performance liquid chromatography, we did not detect any remaining amino acids, indicating that any material still present was likely bound within the frustule. Upon HF dissolution of diatom frustules (yielding the frustule-bound organic carbon), generally 0.02-0.05% of the total hydrolyzable amino acids associated with the diatoms remains (Ingalls et al., 2003).

Any treatment of the samples with solvents, freeze-lysing, or sonication, unavoidably fractured the thin frustules into small fragments. As discussed by Round et al. (1990), this species has an extremely delicate frustule that is often dissolved by standard cleaning procedures such as treatment in acid. Although it was difficult to determine how specific fragments corresponded to different parts of the intact frustule, this fracturing was an unavoidable necessity, since we needed to clean the frustules as thoroughly as possible. In addition, the fragments were thinner than intact frustules (consisting of part of only one valve, instead of both), providing fine-scale resolution of frustule morphology and organic matter distribution that could not be resolved otherwise. To preserve some intact frustules for examination, an additional sample was prepared by boiling cells in 10% sodium dodecyl sulfate (SDS) for 30 min. and then treating them with 2:1 (CH₂)₂Cl₂:MeOH for 30 min. without sonication. This did not remove organic matter as completely, but at least destroyed most surface coatings. In addition, intact diatoms were examined using scanning electron microscopy (SEM). Klaus Kemp of Microlife Services prepared this sample, and Jim Quinn of Stony Brook University operated the SEM.

2.2. X-ray spectromicroscopy

“Soft” X-ray spectromicroscopy provides physical and chemical information based on the absorption of low-energy X-rays (100 – 1000 eV) by a sample. In this energy region, and in particular, between the binding energies of *K*-shell electrons in carbon (~290 eV) and oxygen (~560 eV), organic matter shows strong absorption and phase contrast, whereas water is relatively non-absorbing (Jacobsen, 1999). This enables the imaging and chemical analysis of organic-rich materials. At X-ray photon energies about 10 eV below the absorption edge of carbon (290 eV), or the binding energy required to remove an inner-shell electron, electrons can be promoted to molecular π^* or σ^* orbitals. This produces absorption resonances that depend on the chemical

binding state of the atom. X-ray spectromicroscopy is inferior in resolution compared with scanning and transmission electron microscopy, and in chemical specificity compared with high-performance liquid chromatography and nuclear magnetic resonance spectroscopy (Myneni, 2002; Brandes et al., 2004). Nevertheless, its advantage over many other microscopic and chemical analysis techniques is that it provides combined physical and chemical data (Myneni, 2002; Brandes et al., 2004).

The use of soft X-ray spectromicroscopy to investigate the distribution and composition of organic carbon in environmental samples is relatively new. Recent applications have focused on terrestrial or atmospheric materials such as fulvic and humic acids (Myneni, 2002), interplanetary dust (Flynn et al., 2004), and fossil plant cell walls (Boyce et al., 2002). Brandes et al. (2004) applied X-ray spectromicroscopy to organic carbon in marine samples, comparing the distributions of proteins, carbohydrates, lipids, algaenans, acidic compounds, and black carbon in sediment trap samples from the Arabian Sea. Improved statistical techniques have made such spatial and compositional comparisons possible (Lerotic et al. 2004, 2005). Imaging the organic carbon within diatom frustules is extremely difficult, since the organic constituents are so dilute and the oxygen atoms in silica are strongly absorbing of X-rays at low energies, creating a very low signal over the background absorption. To our knowledge, this study represents the first successful attempt to simultaneously image and obtain chemical information about the organic matter within a diatom frustule using X-ray spectromicroscopy near the carbon edge.

The samples were examined by transmission soft X-ray spectromicroscopy at the X-1A beamline (outboard branch) of the National Synchrotron Light Source (NSLS) facility at Brookhaven National Laboratory. At the NSLS, an undulator produces the X-ray beam, which passes through a monochromator and is focused to a spot using Fresnel zone plates at the X-1A beamline (Feser et al., 2001; Flynn et al., 2004). Samples and all microscope components are kept in

a helium-filled chamber to prevent CO₂, O₂, or N₂ from absorbing X-ray photons (Feser et al., 2000). Further details on X-ray spectromicroscopy, and in particular, on the operation of the X-1A beamline are provided by Jacobsen (1999), Feser et al. (2001) and Flynn et al. (2004).

Scanning transmission X-ray microscopy (STXM) was used to generate a high-resolution (~50 nm) image of each sample. Information on the chemical composition of each sample was obtained simultaneously through X-ray absorption near-edge structure (XANES) spectroscopy near the carbon edge (290eV). Stacks (series of images taken at different energies) were generally conducted starting at a photon energy of about 280 eV and progressing to about 305 – 310 eV. The X-ray photon energy was increased by 0.1 eV increments in the vicinity of the C edge (from ~284-290 eV) and by 0.2 – 0.5 eV at energies away from the edge to minimize the exposure of the samples to the potentially damaging X-ray beam. Each stack of images was digitally aligned, and XANES spectra were generated by calculating the natural logarithm of the ratio in optical density (absorbance) of the sample and background areas. In addition, the distribution of organic carbon in each sample was determined by calculating a ratio of the optical density of images taken below and at the absorption edge for C. This produced a carbon map highlighting areas showing the greatest change in absorbance near the absorption edge.

STXM images were acquired for 44 *C. closterium* samples (usually above and below the C edge for comparison) and 10 silica gel samples. XANES spectroscopy and carbon mapping were performed on 11 of the diatom samples and 3 of the silica gel samples. Results were consistent among samples; most interesting images are depicted here. A spectrum was also collected for pure sodium silicate to determine if silica could produce any peaks mimicking organic matter. The silica produced a constant absorbance over the energy range used to examine the samples.

2.3. Multivariate statistical analyses

The stack data were evaluated using multivariate statistical techniques to roughly assess how the composition of organic matter varied spatially in the samples. These techniques are described in detail by Lerotic et al. (2004, 2005) and will only be summarized here. Each pixel within a sample image can have a slightly unique chemical composition and corresponding XANES spectrum. Principal components analysis (a type of regression analysis) was first used to detect the most common spectral signatures in a sample (e.g., peaks in X-ray absorption at 285 or 288 eV, broad plateaus in absorption after 290 eV, etc.). Cluster analysis was then used to find natural groupings of similar pixels within the sample image according to the relative weights of the principal components (i.e., spectra) they contained (Brandes et al., 2004; Lerotic et al., 2004). When pixels are grouped according to the absolute amount of each principal component they contain, this can create artifacts arising from variations in sample thickness (i.e., thicker regions have more of each component). To eliminate this problem, the cluster analysis was performed using the angle distance measure technique (Lerotic et al., 2005). This technique groups pixels according to their ratios of the principal components (i.e., relative contribution of each spectrum), irrespective of absolute absorbance (which would depend on thickness).

3. Results and Discussion

3.1. Distribution of organic carbon

Observation of untreated *C. closterium* cells by light microscopy revealed fairly uniform pennate cells with long spines on both ends and a total length of $\sim 40 \mu\text{m}$ (Fig. 1). Carbon maps of the untreated and cleaned *C. closterium* frustules indicated that carbon was distributed throughout most or all of each frustule fragment, rather than in discrete patches (Fig. 2). This observation is consistent with the theory that the organic template is a requirement for silica precipitation and an

integral component of the silica matrix. In the SDS-cleaned (Fig. 2a) sample, only large-scale patterning could be observed (looking through the two valves of the frustule simultaneously obscured the fine-scale patterning of the sample). In this sample, carbon seemed to be evenly distributed in proportion to thickness, which is indicated by absorbance below the C edge. Thicker (darker) regions in the STXM image corresponded with more C-rich (brighter) regions in the carbon map. Treatment with H_2O_2 revealed the finer-scale patterning of the frustule (Fig. 2b). At this scale, carbon mostly appeared to be concentrated in thin, highly patterned regions. In the acid-cleaned (Fig. 2c) sample, however, carbon again seemed to be evenly distributed in proportion to thickness. Most likely, hydrolysis of the sample in HCl removed some organic coating that was resistant to H_2O_2 oxidation (and which may have been concentrated in the highly patterned regions with high surface area). This indicates that there were different portions of organic matter (with varying susceptibilities to chemical attack) associated with the frustules. Some organic matter was associated with the internal or external surfaces of the frustule (e.g., as an organic coating or cell wall), but a portion remained even after chemical oxidation and hydrolysis, suggesting it was present internally within the silica matrix itself.

It is still not clear precisely how organic matter and silica are associated in the frustule, but our results are most consistent with the idea that molecules of organic matter and silica are interspersed throughout the frustule. This is suggested by our observations that organic matter was evenly distributed throughout the frustule, was not completely removed by harsh chemical treatments, and that partial removal of this organic matter resulted in partial dissolution and fracturing of the frustule. If organic matter were present as a discrete layer on the external or internal surface of the frustule, it would probably be more vulnerable to chemical attack, and its removal would not disrupt the structural integrity of the frustule as extensively. As suggested by Li and Volcani (1984), the silicella may be permanently incorporated within the frustule during

silica precipitation and become an integral structural component. Since a portion of this organic matter was resistant to chemical attack, it is also likely protected from decomposition in nature. Conversely, silica may be protected from dissolution by the associated organic matter, as previously suggested by Bidle and Azam (1999) and Bidle et al. (2002).

The extent to which silica and organic matter in frustules protect each other from dissolution or decomposition likely depends on other components of the frustule, such as mineral impurities. Previous research (e.g., van Beusekom and Weber, 1995; van Bennekom et al., 1989; van Cappellen and Qiu, 1997) has demonstrated that diatoms sometimes substitute Al for Si in frustules, and that high Al/Si ratios retard frustule dissolution. Consequently, organic matter in frustules with a high Al content may also be protected from decomposition over longer timescales.

The different portions of organic matter associated with the frustule are not necessarily discrete, but may instead be characterized by a continuum of different associations with silica. Rather than having a distinct boundary between the organic portion of the cell wall and silicified frustule, the cell wall may consist of a gradual transition from a less silicified region to a more silicified region. Some of this cell wall material may be vulnerable to chemical attack (e.g., the surface coating that was removed by HCl), whereas some of it may be protected by its association with silica.

3.2. Overall composition of organic carbon

XANES spectra were collected from each sample as a whole to assess the overall composition of biomineral-bound carbon. These spectra displayed resonance peaks near 285 and 288 eV, corresponding to aromatic/unsaturated and carbonyl structures, respectively, and a broad plateau from about 290-295 eV, which is present in the spectra of all organic compounds and corresponds to the C absorption edge and higher resonances (Fig. 3, top line; Müller et al., 1998;

Brandes et al., 2004). The carbonyl peak most likely resulted from carboxylic acid in proteins in the frustules (Kaznatcheyev et al., 2002). Comparison of the frustule spectra with the spectrum for pure polylysine, which also displayed a peak at 288 eV, further supports this explanation (Fig. 3). Proteins usually exhibit carbonyl peaks between 288.0 and 288.3 eV; the presence of amide bonds shifts the carbonyl peak down in energy by 0.2-0.3 eV compared with pure carboxylic acids (Zubavichus et al., 2004; Brandes et al., 2004). Some samples, however, exhibited slightly higher-energy carbonyl peaks (288.4-288.5 eV) more consistent with free organic acids (Figs. 4, 5). These proteins may have been comprised mostly of short chains of amino acids with fewer amide bonds.

The unsaturated or aromatic peak at 285 eV may have been produced by the aromatic amino acids phenylalanine, tryptophan, tyrosine, or histidine (which have aromatic side chains) (Kaznatcheyev et al., 2002) or by aromatic polyamines or sugars. Hydrolysates of HF-dissolved diatom frustules are generally depleted in aromatic amino acids (Hecky et al., 1973; Ingalls et al., 2003); however, the presence of the aromatic peak only indicates that such compounds are present, even if in dilute concentrations.

3.3. Spatial variations in organic carbon composition

Cluster analysis was performed on each sample to detect any spatial heterogeneity in organic compounds within the frustules. Interestingly, different organic constituents appeared to be distributed throughout the frustules in a way that was related to their nanoscale morphology. Figures 4-7 depict the results of cluster analysis for four samples. The first sample depicted (Fig. 4) was freeze-lysed and cleaned with 2:1(CH₂)₂Cl₂:MeOH followed by 30% H₂O₂. The other three samples (Figs. 5-7) were treated in the same manner followed by hydrolysis in 6N HCl at 110°C for 20h. Each figure consists of a STXM image of the sample (a), a composite image of all of the clusters detected (b), and an image and XANES spectrum for each cluster (c-g).

Each sample contained 4-5 different types of material, grouped into clusters by their relative proportions of each principal component. In each sample, the background (c) was free of carbon. The thick portion of the frustule (d) contained carbonyl material (indicated by the peak at about 288 eV) and exhibited a dip just before 285 eV. As described in section 3.2, the carbonyl material was most likely composed of protein. It is not clear what produced the dip; it may represent the trailing end of a lower-energy (< 280 eV) peak from another element. Manual integration of this portion of the frustule produced the same feature, indicating that it was not an artifact of cluster analysis.

The thin, highly patterned regions (e) contained unsaturated or aromatic carbon (indicated by the peak at about 285 eV) as well as carbonyl material. These regions are quite rich in unsaturated carbon, with XANES spectra resembling those of pure aromatic amino acids and other aromatic-rich organic compounds (Cody et al., 1998; Kaznacheyev et al., 2002).

Several additional clusters were apparent. One cluster (f) contained organic material and occasionally (in Figs. 4-6) a small amount of potassium (indicated by the two peaks at 297.1 and 299.8 eV). Finally, three of the samples (Figs. 4-6) exhibited a cluster (g) containing organic material and a larger amount of potassium. It is unlikely that this potassium resulted from the incomplete removal of salts, since the samples were rinsed many times using several different solvents and distilled water. Any organic components of the cell not bound inside the frustule (e.g., potassium-rich ion channels or enzymes in the attached cell wall) would probably have been removed by the organic solvents. This material may have been present within some organic component of the frustule, and consequently survived the harsh sample treatments.

It is interesting that although the total distribution of organic matter may have changed slightly with each of the progressively more stringent sample treatments (as shown in the carbon maps), the bulk composition of this organic matter did not change. Both the H₂O₂ (Fig. 4) and HCl-cleaned samples (Figs. 5-7) contained protein and a similar distribution of saturated and unsaturated

material, indicating the organic constituents of diatom frustules are protected from chemical attack by electrostatic interactions or physical occlusion in the silica. This is an important finding both for carbon preservation in the ocean as well as future studies investigating the composition of organic carbon in diatom frustules.

3.3.1. Relationship with morphological structures

The relationship between the composition of organic matter and frustule morphology in the samples is consistent with the theory that an organic template (e.g., the silicalemma) directs the precipitation and patterning of silica. The reverse is also possible, that as silica precipitates in different morphological patterns, it entrains different organic compounds. However, since other studies (e.g., Mitzutani et al., 1998; Kröger et al., 2000; Noll et al., 2002) have found evidence that organic composition directs silica deposition, the former explanation appears more likely.

To describe how the chemical composition and morphology of the frustules might be related, the physical structure of diatom frustules must be explained. In addition to their larger scale (on the order of several μm) morphological features such as valves and spines, frustules also contain much smaller scale (on the order of several nm) structures that produce the intricate patterning we observed using STXM. In most diatoms, each valve (“lid”) of the silica frustule is perforated by numerous pores called areolae, which are thought to allow solute exchange across the cell membrane (Tomas, 1997). The complexity of these areolae differs among diatom species. In some species, the areolae are simple holes, while in others they are hollow chambers, with a roof, floor, and walls (Round et al., 1990). In many raphid diatoms (those with a longitudinal slit through the frustule), the pores are covered by a delicate layer of silica perforated by numerous smaller pores (Round et al., 1990). Since *C. closterium* is a raphid diatom, and the structures we observed are consistent with a

layer of finely perforated silica covering a larger opening (this is particularly evident in Fig. 4), we suggest that the compositional differences we found were located within the areolae.

The thin, finely-patterned regions of the *C. closterium* frustules (Figs. 4-7e) resemble the perforated roofs covering the pores, whereas the opaque regions of the frustule (Figs. 4-7d) may correspond to the walls between neighboring pores. Our results suggest that aromatic compounds are located in the perforated roofs of these pores, perhaps directing the elaborate, fine-scale structure of the silica there. The scanning electron microscopy (SEM) image in Fig. 8 shows that these pores appear to be distributed throughout the frustule, including along the raphe (slit in the center of the diatom show in Fig. 8b and c), fibrillae (heavily silicified “buttons” at the top and bottom of Fig. 8b), and spine (Fig. 8d). In *C. closterium*, the pores are most prevalent between thin siliceous ribs, or costae, subtending the raphe (Round et al., 1990) (e.g., see the criss-cross pattern apparent in the lower half of Fig. 8b), indicating that most of the samples were likely from this region. In these images, the fine-scale surface structure of the pores (i.e., the finely-patterned lid) could not be resolved since they were obscured by the gold coating.

Assuming that organic constituents of diatom frustules do direct silica deposition, these findings suggest that variations in the composition of this organic matter control nanoscale variations in frustule morphology. This is consistent with the mechanism of silica deposition proposed by Kröger et al. (2000), who argued that interactions between species-specific polyamines and silica-precipitating proteins control the frustule morphologies of different diatom species. Furthermore, the results of this study suggest that these compositional variations not only control morphological differences among species of diatoms, but within the frustule of a single diatom.

If silica molecules are deposited on an organic template, they must do so through chemical interaction with these organic components. More likely, this occurs via electrostatic attraction, since

little evidence has been found for the formation of covalent organo-silicon complexes (Kinrade et al., 2002; Sahai, 2004).

3.3.2. *Alternative explanations*

The exposure of organic matter to high radiation doses can result in beam damage, or a loss of mass and change in the apparent composition of organic matter in a sample (Williams et al., 1993; Zhang et al., 1995; Müller et al., 1998; Beetz and Jacobsen, 2003). Beam damage is an unlikely explanation for the compositional variations observed, however, since the radiation doses to samples in this study were approximately 10^6 Gy, which is below the threshold for observable mass loss in dry biological specimens (Williams et al., 1993). Also, stacks were always conducted starting at lower energies and moving to higher energies to minimize radiation doses at the lower-energy end of the spectrum (280-290 eV). Using the same radiation doses on the same microscope, Kaznatcheyev et al. (1992) found no evidence of beam damage to amino acids, the dominant material in the samples investigated in this study. Also, when beam damage causes a shift towards lower energies, this normally results in the production of several lower-energy peaks (most noticeably around 286.5 eV), as opposed to a single peak at 285 eV (Zhang et al., 1995). Nevertheless, beam damage tests were performed on 5 samples; the results of one of these are shown in Fig. 9. The beam was focused on small regions within a H_2O_2 -cleaned sample and the shutter was opened, allowing full exposure to the X-ray beam. A short stack was then taken over a larger region of the sample. Finally, cluster analysis was used to determine if the composition of organic matter differed in the small areas exposed to the beam as compared with the surrounding region.

The samples contained two clusters (d and e) that were practically indistinguishable, each containing carbonyl carbon and possibly a small amount of unsaturated or aromatic carbon. The samples did not exhibit any variation in the vicinity of the area subjected to beam damage. This

suggests that natural variations in organic matter concentrations, rather than beam damage, produced the observed variations in optical density. This sample was similar in structure to the image shown in Fig. 5, and had approximately the same baseline absorbance ($-\ln I/IO = 0.4$ eV) before correction to zero, indicating these two samples were of comparable thicknesses. Therefore, the sample used in the beam damage test is considered representative of the other samples.

Finally, it is also unlikely that contamination of the samples could have produced the apparent patterns in the presence of unsaturated or aromatic material. Contaminants would have adsorbed onto all regions to some extent (even if they were preferentially concentrated in some regions), but many regions did not contain any of this material. It is possible that the aromatic compounds observed in the pores were an artifact of treatment (e.g., hydrophobic compounds coalescing in a small space due to exposure to aqueous solvents). However, if these compounds were not bound within the silica, we would expect to see at least a small amount present in the background. We checked for any unrecovered amino acids following treatment, and are confident that the rigorous cleaning procedures performed (sonicating in 2:1 MeCl₂:MeOH, oxidation with H₂O₂, followed by hydrolysis in 6N HCl, rinsing 3X in distilled water after each step) removed any organic matter not bound within the silica.

3.4. Comparison between diatom frustules and biomimetic silica gel

The morphological and chemical properties of the synthetic silica gel were similar to those of the diatom frustules (compare Fig. 10 with Figs. 4-7). Also, the fine-scale morphology of the frustules and gel appear to be consistent with the general nanostructure of biogenic silica observed under scanning electron and atomic force microscopy by previous researchers (Kröger et al., 2002; Noll et al., 2002; Sumper, 2002). XANES analysis of the gel indicated that it contained organic matter (primarily carboxyl carbon), consistent with lysine incorporation. A XANES spectrum of the

pure silicic acid used to prepare the gel did not reveal any organic peaks, indicating that the peaks observed in the gel were produced by the polylysine added, and not by contamination. The morphological and chemical similarities between the gel and frustules support the hypothesis that organic compounds direct the precipitation of silica in diatom frustules.

Furthermore, since treatment of the gel with H_2O_2 and 6N HCl failed to remove at least part of this organic matter, it would appear that the polylysine did not merely catalyze silica precipitation, but became incorporated within the gel as it formed. This is a tentative conclusion, since the results of subsequent experiments (unpublished) suggest that a large fraction of polylysine eventually diffuses out of the gel or is released by dissolution of the silica (losses of ~60-75% after 3 days, and ~88-98% after 84 days were observed).

4. Conclusions

Soft X-ray spectromicroscopy is a promising technique with a variety of applications in environmental science. The use of this technique in conjunction with multivariate statistical analyses can help elucidate spatial variations in the composition of organic matter in natural samples.

The results of this study are consistent with the theory that the organic constituents of diatom frustules direct their nanoscale patterning, and that this organic matter is protected from chemical attack once incorporated in the shell. The relationship between organic matter composition and silica morphology, the failure of harsh chemical treatments to remove all of this organic matter, and the spontaneous nature of the co-precipitation of silica and organic matter indicate some level of chemical interaction between the siliceous and organic components of diatom frustules. Although some surface coatings or cell wall material may be subject to chemical attack, this biomineral-bound organic matter should be protected against decomposition until the mineral

dissolves. Furthermore, paleoceanographic techniques using diatom-bound organic matter as proxies of past environmental changes should be extremely reliable.

Acknowledgements

We would like to thank Mirna Lerotic, who was instrumental in developing the statistical tools used in this study and who provided considerable assistance with our data analysis. We would also like to thank Anitra Ingalls, whose research on the preservation of biomineral-bound proteins paved the way for this study. The X-1A scanning transmission X-ray microscope used in this study was developed by the group of Janos Kirz and Chris Jacobsen at Stony Brook University, and the zone plates were developed by Steve Spector and Chris Jacobsen of Stony Brook and Don Tennant of Lucent Technologies Bell Labs. Shelagh Palma of Nicholas Fisher's laboratory provided assistance culturing the diatoms. Bassem Allam and Sue Pawagi provided assistance with light microscopy. Klaus Kemp of Microlife Services prepared the samples for scanning electron microscopy (SEM), and Jim Quinn operated the SEM. This study was supported by NSF grants OCE0136370 (C. Lee) and OCE0117062 (R. Aller). This is MSRC contribution number 1353 and MedFlux contribution number 14.

References

- Armstrong, R.A., Lee, C., Hedges, J.I., Honjo, S., Wakeham, S.G., 2002. A new, mechanistic model for organic carbon fluxes in the ocean based on the quantitative association of POC with ballast minerals. *Deep-Sea Research II* 49, 219-236.
- Beetz, T., Jacobsen, C., 2003. Soft X-ray radiation-damage studies in PMMA using a cryo-STXM. *Journal of Synchrotron Radiation* 10, 280-283.
- Bidle, K., Azam, F., 1999. Accelerated silica dissolution by marine bacterial assemblages. *Nature* 397, 508-512.
- Bidle, K., Manganello, M., Azam, F., 2002. Regulation of ocean silicon and carbon preservation by temperature control on bacteria. *Science* 298, 1980-1984.
- Boyce, C., Cody, G., Feser, M., Jacobsen, C., Knoll, A., Wirick, S., 2002. Organic chemical differentiation within fossil plant cell walls detected with X-ray spectromicroscopy. *Geology* 30, 1039-1042.
- Brandes, J.A., Lee, C., Wakeham, S., Peterson, M., Jacobsen, C., Wirick, S., Cody, G., 2004. Examining marine particulate organic matter at sub-micron scales using scanning transmission X-ray microscopy and carbon X-ray absorption near edge structure spectroscopy. *Marine Chemistry* 92, 107-121.
- Cha, J.N., Shimizu, K., Zhou, Y., Christiansen, S.C., Chmelka, B.F., Stucky, G.D., Morse, D.E., 1999. Silicatein filaments and subunits from a marine sponge direct the polymerization of silica and silicones in vitro. *Proceedings of the National Academy of Sciences* 96, 361-365.
- Cody, G.D., Ade, H., Wirick, S., Mitchell, G.D., Davis, A., 1998. Determination of chemical-structural changes in vitrinite accompanying luminescence alteration using C-NEXAFS analysis. *Organic Geochemistry* 28, 441-455.

- Feser, M., Beetz, T., Carlucci-Dayton, M., Jacobsen, C., 2000. Instrumentation advances and detector development with the Stony Brook scanning transmission X-ray microscope. In: X-ray Microscopy: Proceedings of the Sixth International Conference (eds. W. Meyer-Ilse, A. Warwick and D.T. Attwood). American Institute of Physics, Melville, New York. pp. 367-372. (Also available at <http://xray1.physics.sunysb.edu/research/publications.php>)
- Feser, M., Beetz, T., Carlucci-Dayton, M., Jacobsen, C., 2001. Scanning transmission soft X-ray microscopy at beamline X-1A at the NSLS - advances in instrumentation and selected applications. In: Soft X-ray and EUV Imaging Systems II (eds. D.A. Tichenor and J.A. Folta). Society of Photo-Optical Instrumentation Engineers, Bellingham, Washington. pp. 146-153. (Also available at <http://xray1.physics.sunysb.edu/research/publications.php>)
- Flynn, G.J., Keller, L.P., Jacobsen, C., Wirick, S., 2004. An assessment of the amount and types of organic matter contributed to the Earth by interplanetary dust. *Advances in Space Research* 33, 57-66.
- Hecky, R.E., Mopper, K., Kilham, P., Degens, E.T., 1973. The amino acid and sugar composition of diatom cell-walls. *Marine Biology* 19, 323-331.
- Ingalls, A.E., Lee, C., Wakeham, S.G., Hedges, J.I., 2003. The role of biominerals in the sinking flux and preservation of amino acids in the Southern Ocean along 170°W. *Deep-Sea Research II* 50, 709-734.
- Ingalls, A.E., Anderson, R.F., Pearson, A., 2004. Radiocarbon dating of diatom-bound organic compounds. *Marine Chemistry* 92, 91-105.
- Jacobson, C., 1999. Soft X-ray microscopy. *Trends in Cell Biology* 9, 44-47.
- Kaznatcheyev, K., Osanna, A., Jacobsen, C., Plashkevych, O., Vahtras, O., Ågren, H., Carravetta, V., Hitchcock, A.P., 2002. Innershell absorption spectroscopy of amino acids. *Journal of Physical Chemistry A* 106, 3153-3168.

- King, K.J., 1974. Preserved amino acids from silicified protein in fossil Radiolaria. *Nature* 252, 690-692.
- Kinrade, S.D., Gillson, A.M.E., Knight, C.T.G., 2002. Silicon-29 NMR evidence of a transient hexavalent silicon complex in the diatom *Navicula pelliculosa*. *Journal of the Chemical Society – Dalton Transactions* 3, 307-309.
- Klaas, C., Archer, D. E., 2002. Association of sinking organic matter with various types of mineral ballast in the deep sea: Implications for the rain ratio. *Global Biogeochemical Cycles* 16, 1116, doi:10.1029/2001GB001765.
- Kröger, N., Deutzmann, R., Sumper, M., 1999. Polycationic peptides from diatom biosilica that direct silica nanosphere formation. *Science* 286, 1129-1132.
- Kröger, N., Deutzmann, R., Bergdorf, C. Sumper, M., 2000. *Proceedings of the National Academy of Sciences* 97, 14133-14138.
- Kröger, N., Lorenz, S., Brunner, E. Sumper, M., 2002. Self-assembly of highly phosphorylated silaffins and their function in biosilica morphogenesis. *Science* 298, 584-586.
- Lerotic, M., Jacobsen, C., Gillow, J.B., Francis, A.J., Wirick, S., Vogt, S. Maser, J., 2005. Cluster analysis of soft X-ray spectromicroscopy: finding the patterns in complex specimens. *Journal of Electron Spectroscopy and Related Phenomena* 144-147C, 1137-1143. (Also available at <http://xray1.physics.sunysb.edu/research/publications.php>)
- Lerotic, M., Jacobsen, C., Schäfer, T. Vogt, S., 2004. Cluster analysis of soft X-ray microscopy data. *Ultramicroscopy* 100, 35-57.
- Li, C.W., Volcani, B.E., 1984. Aspects of silicification in wall morphogenesis of diatoms. *Philosophical Transactions of the Royal Society of London B* 304, 519-528.
- Martin-Jézéquel, V., Hildebrand, M. Brzezinski, M.A., 2000. Silicon metabolism in diatoms: implications for growth. *Journal of Phycology* 36, 821-840.

- Mitzutani, T., Nagase, H., Fujiwara, N., Ogoshi, H., 1998. Silicic acid polymerization catalyzed by amines and polyamines. *Bulletin of the Chemical Society of Japan* 71, 2017-2022.
- Müller, H.U., Zharnikov, M., Völkel, B., Schertel, A., Harder, P., Grunze, M., 1998. Low-energy electron-induced damage in hexadecanethiolate monolayers. *Journal of Physical Chemistry B* 102, 7949-7959.
- Myneni, S.C.B., 2002. Soft X-ray spectroscopy and spectromicroscopy studies of organic molecules in the environment. In: Fenter, P., Rivers, M., Sturchio, N., Sutton, S (Eds.), *Reviews in Mineralogy and Geochemistry* 49, Applications of Synchrotron Radiation in Low-Temperature Geochemistry and Environmental Science, pp. 485-571.
- Noll, F., Sumper, M., Hampp, N., 2002. Nanostructure of diatom silica surfaces and of biomimetic analogs. *Nano Letters* 2, 91-95.
- Robbins, L.L., Brew, K., 1990. Proteins from the organic matrix of core-top and fossil planktonic foraminifera. *Geochimica et Cosmochimica Acta* 54, 2285-2292.
- Round, F.E., Crawford, R.M., Mann, D.G., 1990. *The Diatoms: Biology and Morphology of the Genera*. Cambridge University Press, Cambridge, England.
- Sahai, N., 2004. Calculation of ^{29}Si shifts of silicate complexes with carbohydrates, amino acids, and $\mu\text{Hicarboxylic}$ acids: potential role in biological silica utilization. *Geochimica et Cosmochimica Acta* 68, 227-234.
- Sigman, D.M., Altabet, M.A., Francois, R., McCorkle, D.C., Gaillard, J.F., 1999. The isotopic composition of diatom-bound nitrogen in Southern Ocean sediments. *Paleoceanography* 14, 118-134.
- Sigman, D.M., Boyle, E.A., 2000. Glacial/interglacial variations in atmospheric carbon dioxide. *Nature* 407, 859-869.

- Abramson et al., X-ray Spectromicroscopy of Diatom Frustules
- Sumper, M., 2002. A phase separation model for the nanopatterning of diatom biosilica. *Science* 295, 2430-2433.
- Swift, D.M. and Wheeler, A.P., 1992 Evidence of an organic matrix from diatom biosilica. *Journal of Phycology* 28, 202-209.
- Tomas, C.R. (ed.), 1997. *Identifying Marine Phytoplankton*. Academic Press, San Diego.
- van Bennekom, A.J., Jansen, J.H.F., van der Gaast, S.J., van Iperen, J.M., Pieters, J., 1989. Aluminum-rich opal: an intermediate in the preservation of biogenic silica in the Zaire (Congo) deep-sea fan. *Deep-Sea Research* 36, 173-190.
- van Beusekom, J.E.E., Weber, A., 1995. Der einfluß von aluminium auf das wachstum und die entwicklung von kieselalgen in der Nordsee. *Deutsche Hydrographische Zeitschrift (German Journal of Hydrography) Supplement 5*. Hamburg and Rostock, Germany, pp. 213-220.
- van Cappellan, P., Qiu, L., 1997. Biogenic silica dissolution in sediments of the Southern Ocean. I: Solubility. *Deep-Sea Research II* 44, 1109-1128.
- Volcani, B.E., 1981. Cell wall formation in diatoms: morphogenesis and biochemistry. In: Simpson, T.L., Volcani, B.E. (Eds.), *Silicon and siliceous structures in biological systems*. Springer-Verlag, New York, pp. 157-200.
- Weiner, S., Erez, J., 1984. Organic matrix of the shell of the foraminifer, *Heterostegina depressa*. *Journal of Foramineral Research* 14, 206-212.
- Williams, S., Zhang, X., Jacobsen, C., Kirz, J., Lindaas, S., Van't Hof, J., Lamm S.S., 1993. Measurements of wet metaphase chromosomes in the scanning transmission x-ray microscope. *Journal of Microscopy* 170, 155-165.
- Zhang, X., Jacobsen, C., Lindaas, S., Williams, S., 1995. Exposure strategies for polymethyl methacrylate from in situ x-ray absorption near edge structure spectroscopy. *Journal of Vacuum Science and Technology B* 13, 1477-1483.

Abramson et al., X-ray Spectromicroscopy of Diatom Frustules

Zubavichus, Y., Fuchs, O., Weinhardt, L., Heske, C., Umbach, E., Denlinger, J.D., Grunze, M.,

2004. Soft X-Ray-Induced Decomposition of Amino Acids: An XPS, Mass Spectrometry, and NEXAFS Study. *Radiation Research* 161, 346-358.

Figure Captions

Figure 1. Image of untreated *C. closterium* cells observed under 1000X magnification using light microscopy. The diatoms were $\sim 15 \mu\text{m}$ pennate cells with long spines on either end, resulting in a total length of $\sim 40 \mu\text{m}$. Valvar (looking down on one valve, or “lid” of the frustule) and apical (looking down on one side of the frustule, where the two valves intersect) planes of view are indicated by crossbars.

Figure 2. Carbon maps of *Cylindrotheca closterium* frustules. The left panels are images of the samples observed under STXM and the right panels are carbon maps. In the carbon maps, the distribution of organic carbon (shown in white) was obtained by taking the ratio of images acquired at different energies (280-283 vs. 293-296 eV) and mapping out the areas that exhibited the greatest change in absorbance just below the carbon absorption edge (290 eV). a: Whole frustule boiled in 10% SDS followed by 2:1 $(\text{CH}_2\text{Cl}_2:\text{MeOH})$. Carbon loadings (indicated by brightness in carbon map) appear to be proportional to sample thickness. b: Fragment produced by freeze-lysing diatoms and then cleaning them with 2:1 $(\text{CH}_2\text{Cl}_2:\text{MeOH})$ followed by 30% H_2O_2 . The elongated, curved appearance of this fragment suggests that it may have originally been located at the intersection of the valvar (surface, or looking down on one valve) and apical (side) planes of view of the frustule (see box in Fig. 1). Lines are provided to indicate alignment of features. Thin, patterned regions (pointed out by lines) appear to have high carbon content. c: Fragments prepared as in sample b and then hydrolyzed in 6N HCl. As in a, carbon loadings appear to be proportional to sample thickness.

Figure 3. XANES carbon spectrum of *C. closterium* frustule (cleaned with 2:1(CH)₂Cl₂:MeOH and H₂O₂) compared with that of a pure polylysine standard. Presence of carbonyl peak (denoted by C=O) in both samples suggests chemical similarity between polylysine and the organic matter present in the diatom frustule. The x-axis is X-ray energy (eV) and the y-axis is -ln of the ratio in absorbance of the sample (I) and background (IO).

Figure 4. Results of cluster analysis on fragment of *C. closterium* frustule. Sample was freeze-lysed and cleaned with 2:1(CH)₂Cl₂:MeOH followed by 30% H₂O₂. The top left panel (a) is an image of the sample observed under STXM. The top right panel (b) depicts the clusters detected by cluster analysis. Five clusters were apparent. Images of each cluster are provided (c-g) with XANES spectra to right. The background (c) contained no carbon. The thick, solid regions of the frustule (d) contained carbonyl material (denoted by C=O). The thin, highly patterned regions (e) contained unsaturated or aromatic carbon (denoted by C=C) as well as carbonyl material. An additional cluster was present containing organic material, possibly with a small amount of potassium (f). A fifth cluster was present containing organic material and a larger amount of potassium (g). The x-axis is X-ray energy (eV) and the y-axis is -ln of the ratio in absorbance of the sample (I) and background (IO).

Figure 5. Results of cluster analysis on fragments of *C. closterium* frustule. The flat appearance of the fragments suggest that they may have originally part of one of the valves of the frustule (see box in Fig. 1). Sample was freeze-lysed, cleaned with 2:1(CH)₂Cl₂:MeOH, with 30% H₂O₂, and finally, hydrolyzed in 6N HCl at 110°C for 20 h. Panels (a-g) are as described in Fig. 4.

Figure 6. Results of cluster analysis on fragments of *C. closterium* frustule. Sample was freeze-lysed, cleaned with 2:1(CH₂)₂Cl₂:MeOH, with 30% H₂O₂, and finally, hydrolyzed in 6N HCl at 110°C for 20 h. Panels (a-g) are as described in Fig. 4.

Figure 7. Results of cluster analysis on fragment of *C. closterium* frustule. Sample was freeze-lysed, cleaned with 2:1(CH₂)₂Cl₂:MeOH, with 30% H₂O₂, and finally, hydrolyzed in 6N HCl at 110°C for 20 h. Panels (a-f) are as described in Fig. 4.

Figure 8. SEM images of *C. closterium*. a) Overview of a cell taken at 5000x magnification. b) Image taken at 50,000x magnification showing small pores located along fibrulae (heavy silicified “buttons” at top and bottom of image and raphe (slit in center of frustule), indicated with boxes. Criss-cross pattern throughout the lower portion of the frustule may also be due to presence of pores. c) Image taken at 100,000x magnification showing pores along raphe. d) Image taken at 50,000x showing pores at the end of the spine. Pores were present throughout both spines.

Figure 9. Beam damage test on fragment of *C. closterium* frustules. Sample was freeze-lysed and then cleaned with 2:1(CH₂)₂Cl₂:MeOH followed by 30% H₂O₂. Top left panel (a) depicts an image of the sample observed under STXM. Boxes indicate regions subjected to beam damage (area where shutter was opened, allowing full exposure to beam). Top right panel (b) depicts clusters detected by cluster analysis. Three clusters were apparent. Images of each cluster are provided (c-f) with XANES spectra to right. The background (c) contained no carbon. Two clusters (d and e) were very similar, primarily containing carbonyl carbon with some unsaturated or aromatic carbon. X-axis depicts X-ray energy (eV) and y-axis depicts $-\ln$ of the ratio in absorbance of the image (I) and background (IO).

Figure 10. Results of cluster analysis on synthetic silica gel prepared by adding polylysine to a buffered solution of silicic acid. Following preparation, the sample was cleaned with 30% H₂O₂ and then hydrolyzed in 6N HCl. The top left panel (a) is an image of the sample observed under STXM and the top right (b) depicts the clusters detected by cluster analysis. Two clusters were apparent. Images of each cluster are provided (c-d) with XANES spectra to right. The background (c) contained no carbon. The gel (d) contained carbonyl material and possibly a small amount of unsaturated or aromatic carbon. The x-axis is X-ray energy (eV) and the y-axis is $-\ln$ of the ratio in absorbance of the sample (I) and background (IO).

Figures



Figure 1

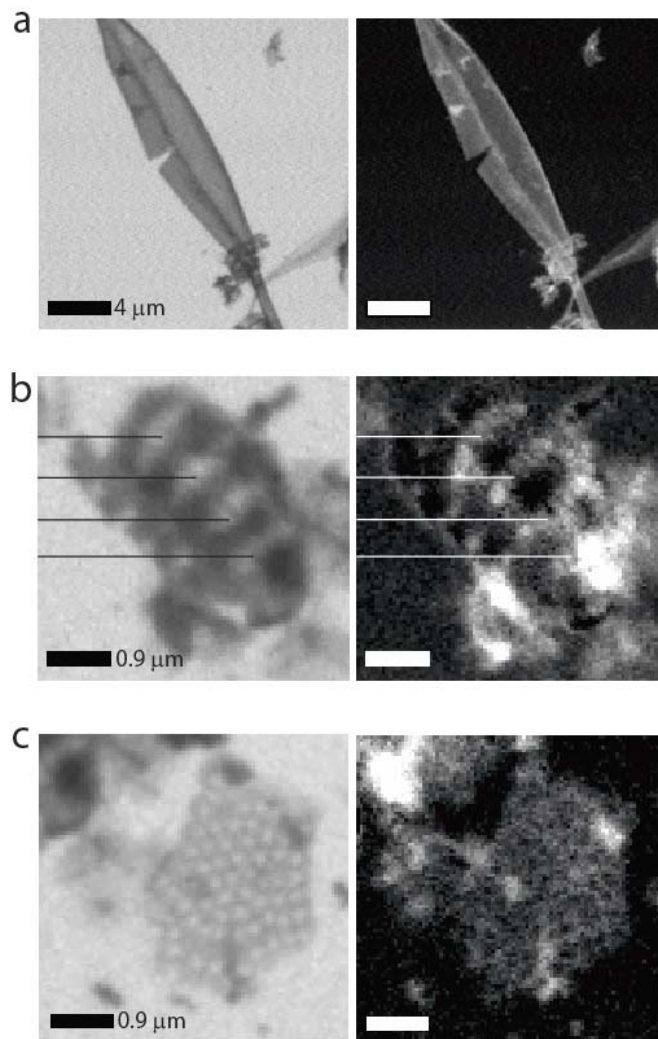


Figure 2

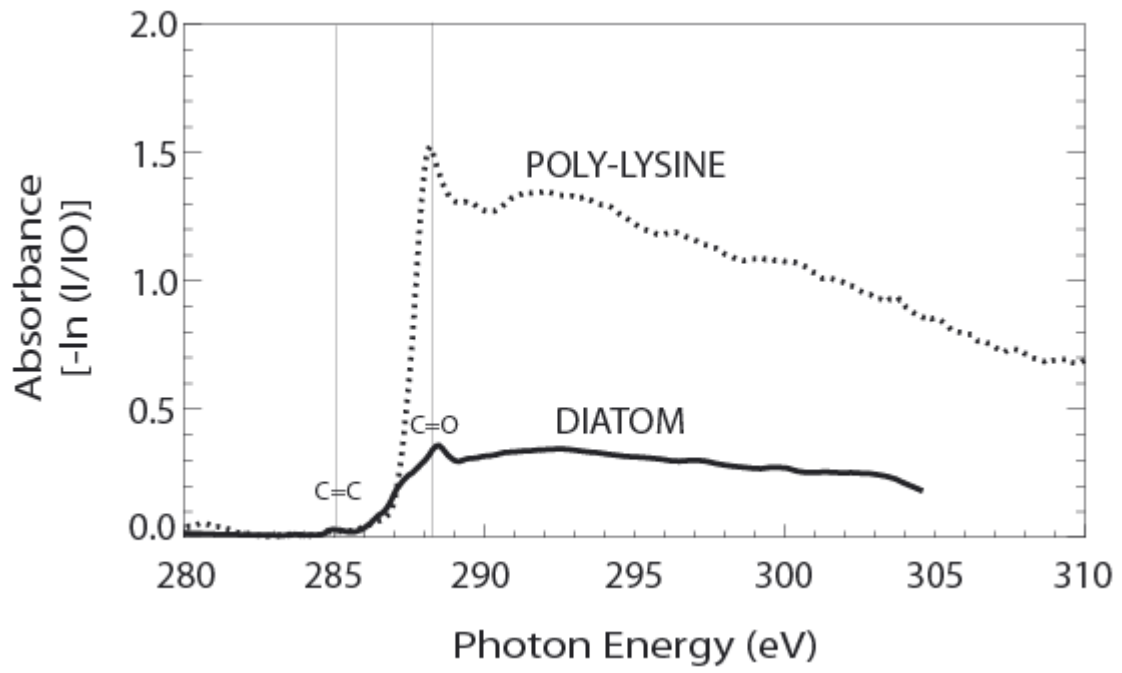


Figure 3

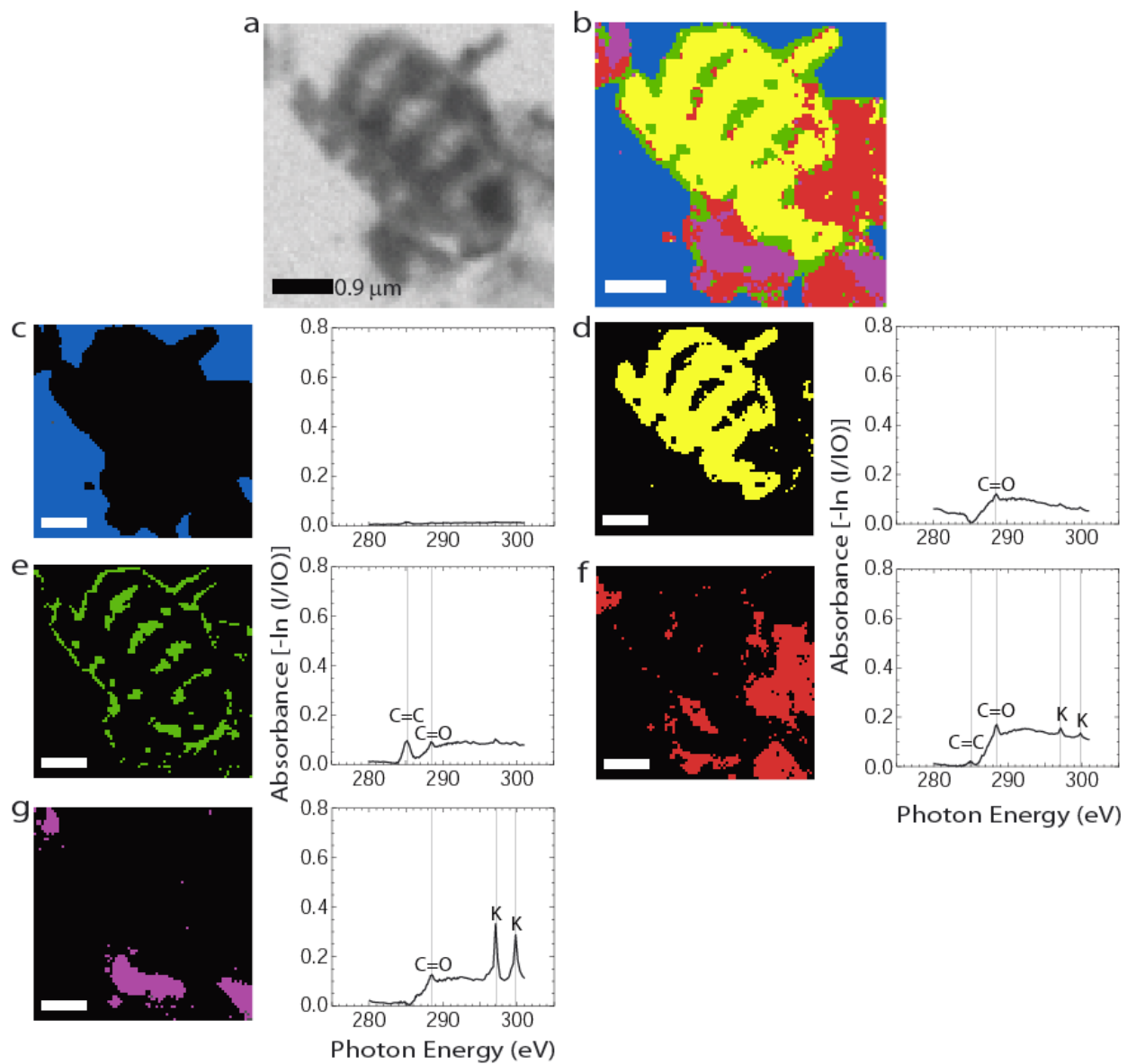


Figure 4

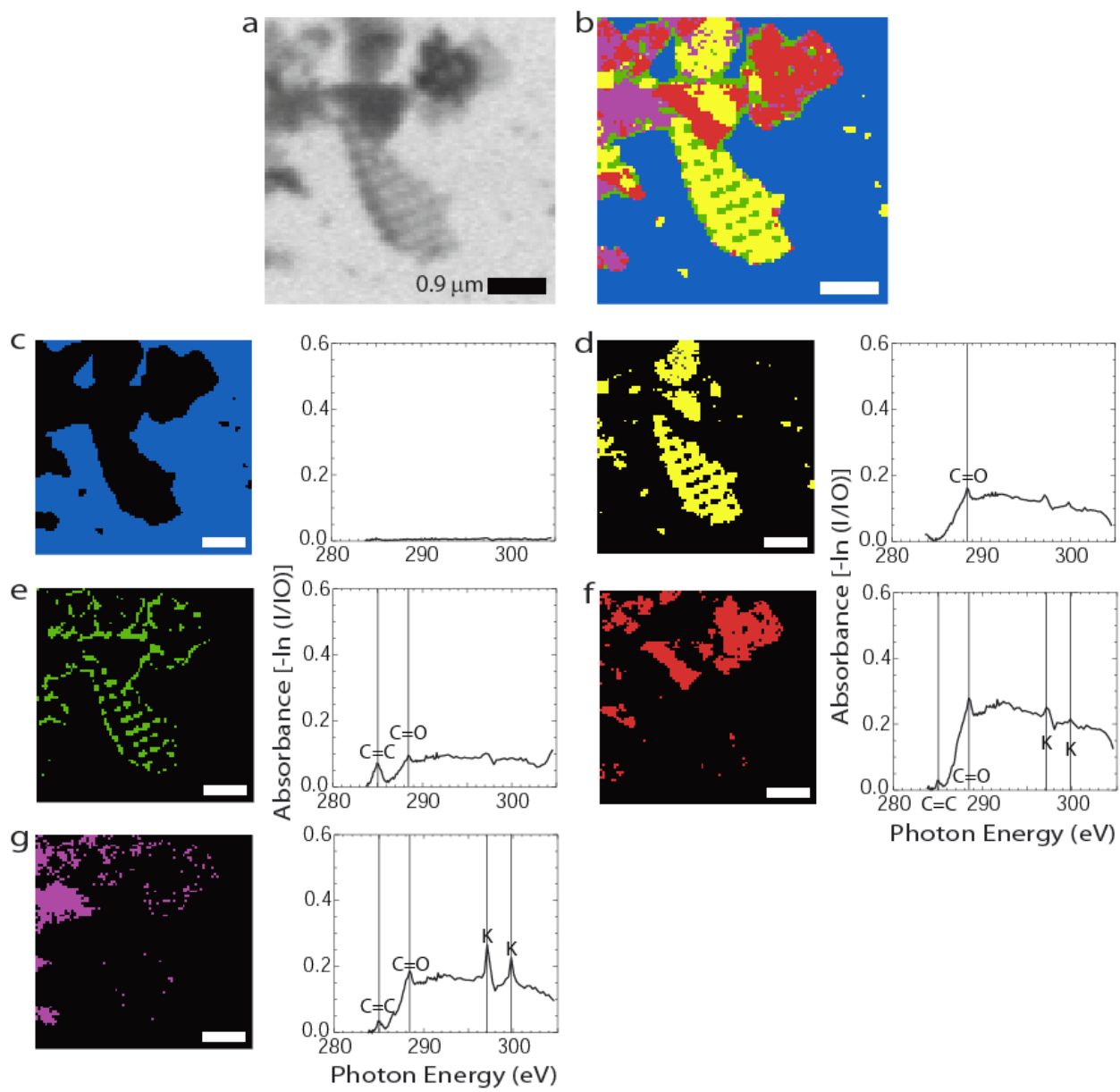


Figure 5

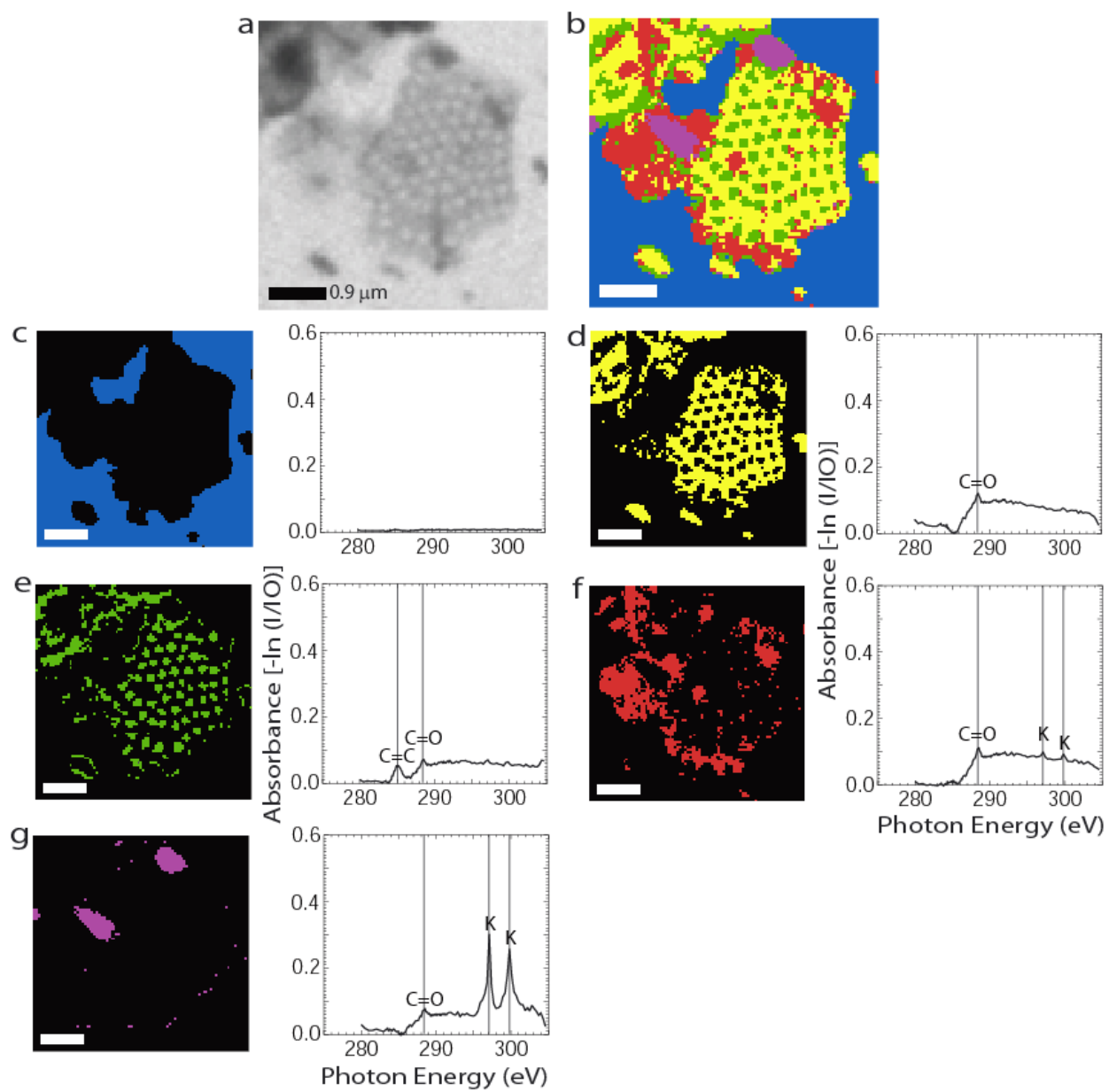


Figure 6

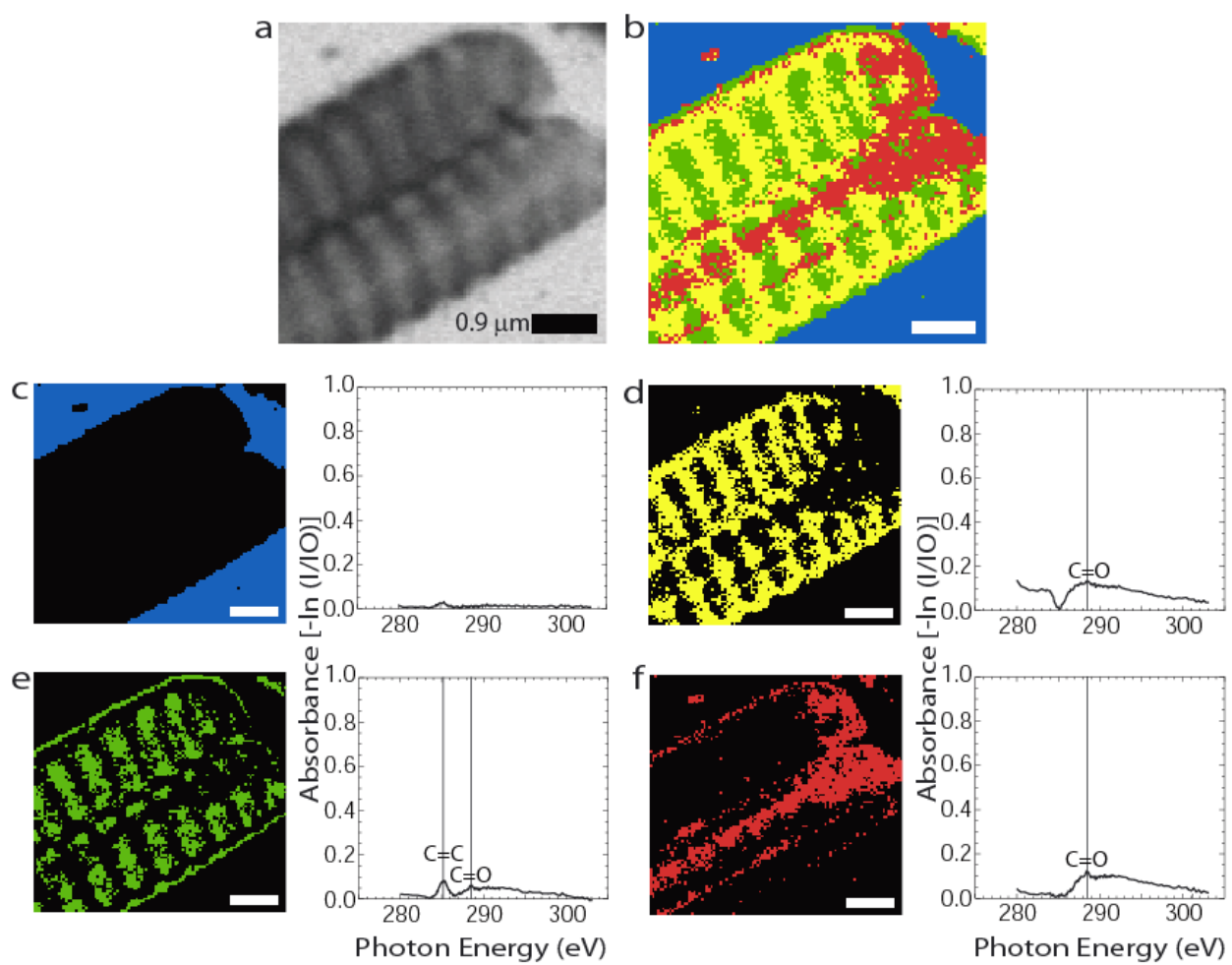


Figure 7

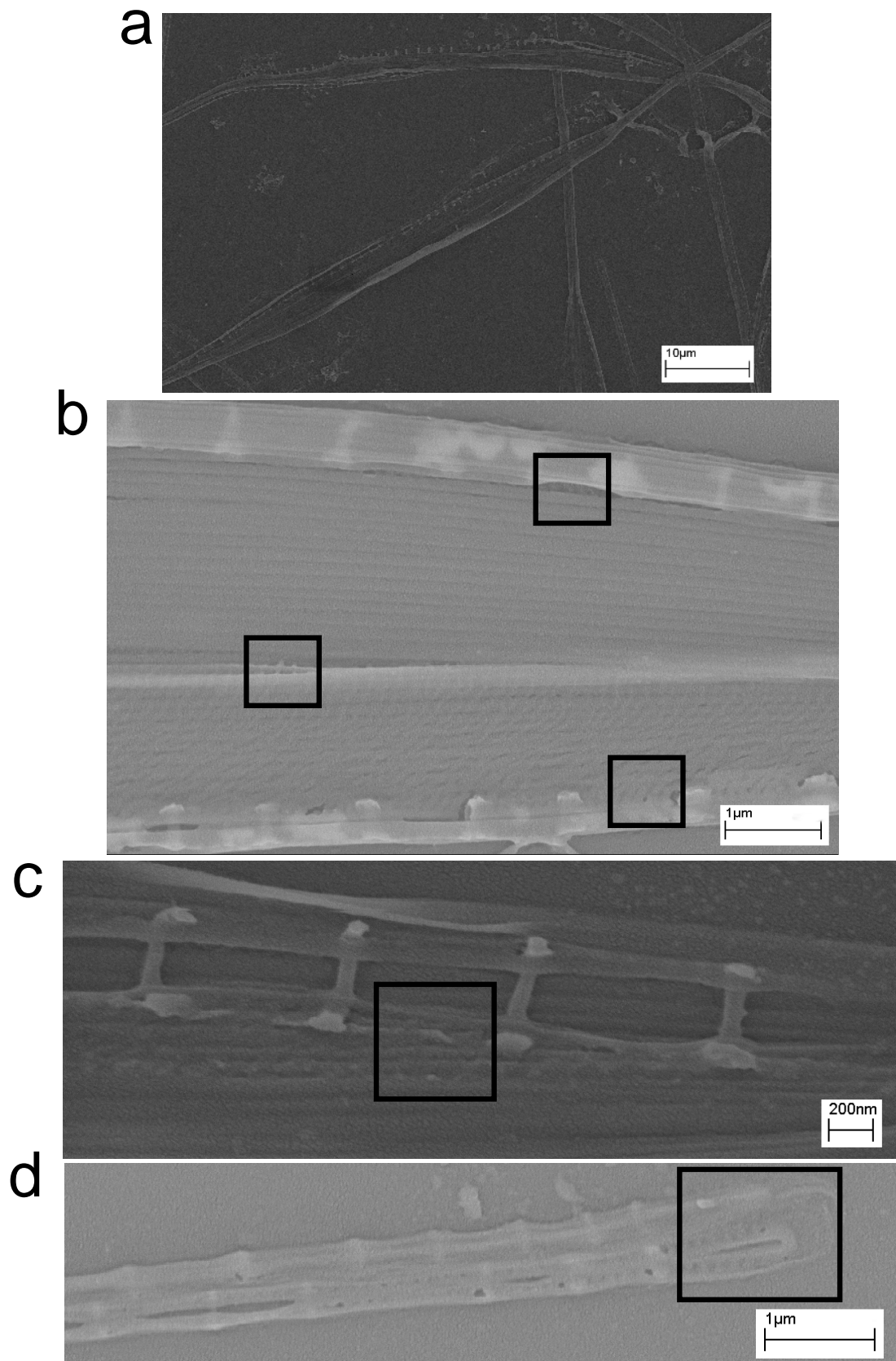


Figure 8

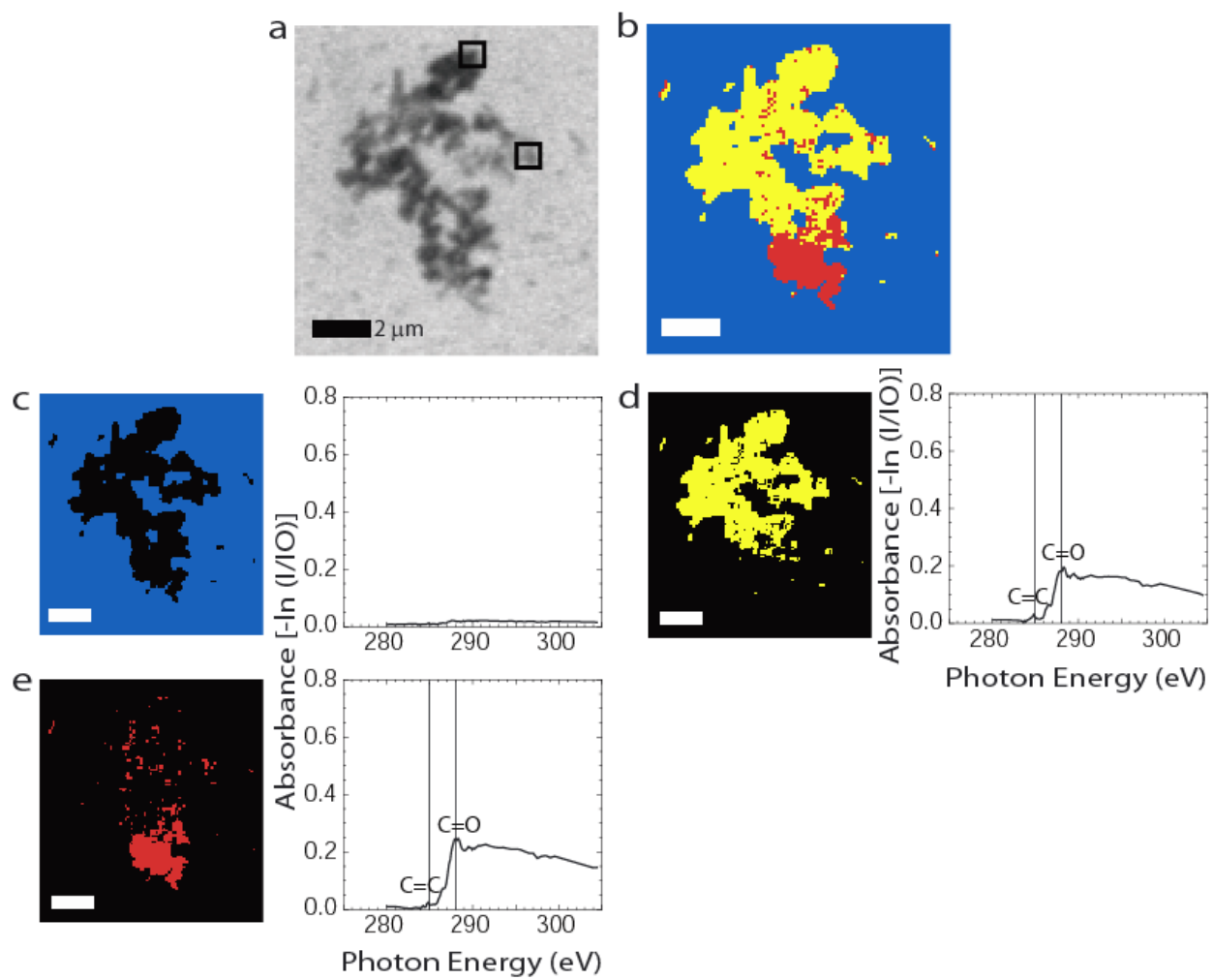


Figure 9

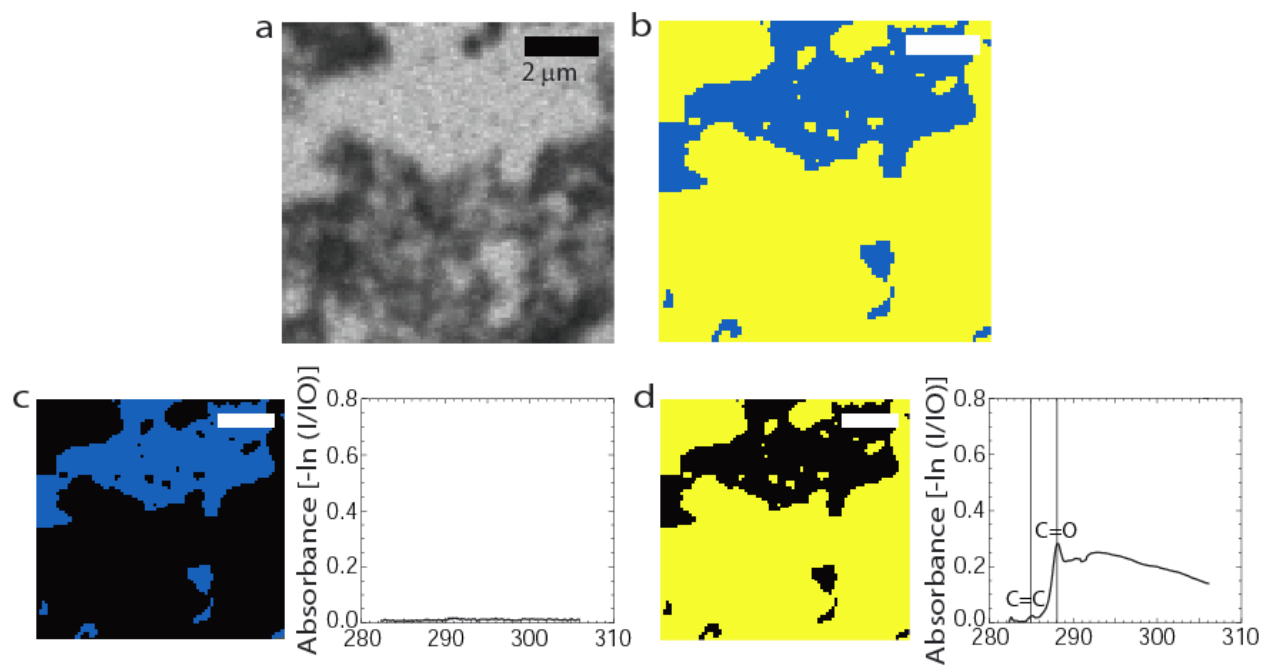


Figure 10